REPORT DOCUMENTATION PAGE

Form Approved OMB NO. 0704-0188

1. REPORT DATE (DD-MM-YYYY)	2. REPORT TYPE	3. DATES COVERED (From - To)
	New Reprint	-

4. TITLE AND SUBTITLE

A COMPUTATIONAL INVESTIGATION OFIMPACT INTO MULTI-PLIES OF PLAIN-WOVEN FABRIC

5a. CONTRACT NUMBER
W911NF-09-1-0513

5b. GRANT NUMBER

5c. PROGRAM ELEMENT NUMBER
622105

6. AUTHORS

M. Grujicic, W. C. Bell, T. He, G. Arakere, B. A. Cheeseman, K. L. Koudela, J. F. Tarter

5d. PROJECT NUMBER

5e. TASK NUMBER

5f. WORK UNIT NUMBER

7. PERFORMING ORGANIZATION NAMES AND ADDRESSES

Clemson University
Office of Sponsored Programs
300 Brackett Hall
Clemson, SC 29634 -5702

8. PERFORMING ORGANIZATION REPORT NUMBER

9. SPONSORING/MONITORING AGENCY NAME(S) AND ADDRESS(ES)

U.S. Army Research Office
P.O. Box 12211
Research Triangle Park, NC 27709-2211

10. SPONSOR/MONITOR'S ACRONYM(S)
ARO

11. SPONSOR/MONITOR'S REPORT NUMBER(S)
56526-EG.2

12. DISTRIBUTION AVAILIBILITY STATEMENT

Approved for public release; distribution is unlimited.

13. SUPPLEMENTARY NOTES

The views, opinions and/or findings contained in this report are those of the author(s) and should not contrued as an official Department of the Army position, policy or decision, unless so designated by other documentation.

14. ABSTRACT

To overcome the high computational cost associated with explicit representation of the fabricyarn weaving structure/architecture in fabric-based flexible personnel protection, a meso-scale unit-cell based material model is first developed for a prototypical plain-woven Kevlar® 129 single-ply fabric. The model is next implemented into a “user-defined material” subroutine and coupled with the ABAQUS/Explicit commercial finite-element program. Within the user defined

15. SUBJECT TERMS

Armor Technology; Impact Damage; Stitched Composites

16. SECURITY CLASSIFICATION OF:			17. LIMITATION OF ABSTRACT	15. NUMBER OF PAGES	19a. NAME OF RESPONSIBLE PERSON
a. REPORT	b. ABSTRACT	c. THIS PAGE			Mica Grujicic
UU	UU	UU	UU		19b. TELEPHONE NUMBER 864-656-5639

Report Title

A COMPUTATIONAL INVESTIGATION OFIMPACT INTO MULTI-PLIES OF PLAIN-WOVEN FABRIC

ABSTRACT

To overcome the high computational cost associated with explicit representation of the fabricyarn weaving structure/architecture in fabric-based flexible personnel protection, a meso-scale unit-cell based material model is first developed for a prototypical plain-woven Kevlar® 129 single-ply fabric. The model is next implemented into a “user-defined material” subroutine and coupled with the ABAQUS/Explicit commercial finite-element program. Within the user defined material subroutine, an effective “smeared” material response is computed which includes not only the in-plane phenomena (e.g. yarn tension, buckling, inter-yarn friction, and yarn slip), but also the out-of-plane effects (e.g. contact forces at the yarn crossovers, and fabric bending and twisting). The material model is next validated by caring out a series of transient non-linear dynamics finite-element analyses of impact of a single-layer fabric by a high-speed spherical steel projectile and by comparing the results with their counterparts obtained in the corresponding computational analyses in which yarns and their weaving is represented explicitly. Finally, the model is used in an investigation of the ability of a multi-ply soft-body armor vest to protect the wearer from impact by a 9mm round nose projectile. The effects of inter-ply friction, projectile/yarn friction and the far-field boundary conditions are revealed and the results explained using simple wave mechanics principles, high-deformation rate material behavior and the role of various energy absorbing mechanisms in the fabric-based armor systems.

REPORT DOCUMENTATION PAGE (SF298)
(Continuation Sheet)

Continuation for Block 13

ARO Report Number 56526.2-EG
A COMPUTATIONAL INVESTIGATION OFIMPA ...

Block 13: Supplementary Note

Approved for public release; distribution is unlimited.

A COMPUTATIONAL INVESTIGATION OF IMPACT INTO MULTI-PLIES OF PLAIN-WOVEN FABRIC

M. Grujicic, W. C. Bell, T. He, G. Arakere
Department of Mechanical Engineering
Clemson University, Clemson SC 29634

B. A. Cheeseman
Army Research Laboratory – Survivability Materials Branch
Aberdeen, Proving Ground, MD 21005-5069

K. L. Koudela, J. F. Tarter
Applied Research Laboratory
The Pennsylvania State University, State College, PA

ABSTRACT

To overcome the high computational cost associated with explicit representation of the fabric-yarn weaving structure/architecture in fabric-based flexible personnel protection, a meso-scale unit-cell based material model is first developed for a prototypical plain-woven Kevlar® 129 single-ply fabric. The model is next implemented into a "user-defined material" subroutine and coupled with the ABAQUS/Explicit commercial finite-element program. Within the user defined material subroutine, an effective "smeared" material response is computed which includes not only the in-plane phenomena (e.g. yarn tension, buckling, inter-yarn friction, and yarn slip), but also the out-of-plane effects (e.g. contact forces at the yarn crossovers, and fabric bending and twisting). The material model is next validated by caring out a series of transient non-linear dynamics finite-element analyses of impact of a single-layer fabric by a high-speed spherical steel projectile and by comparing the results with their counterparts obtained in the corresponding computational analyses in which yarns and their weaving is represented explicitly. Finally, the model is used in an investigation of the ability of a multi-ply soft-body armor vest to protect the wearer from impact by a 9mm round nose projectile. The effects of inter-ply friction, projectile/yarn friction and the far-field boundary conditions are revealed and the results explained using simple wave mechanics principles, high-deformation rate material behavior and the role of various energy absorbing mechanisms in the fabric-based armor systems.

KEY WORDS: Armor Technology; Impact Damage; Stitched Composites

1. INTRODUCTION

Flexible lightweight materials have been used historically in personnel protection systems to provide protection against specified threats, at reduced weight and without compromising person's mobility. Early materials used included leather, silk, metal chain mail and metal plates. Replacement of metal with a nylon (*poly-amide)* fabric and an E-glass fiber/ethyl cellulose composite in body armor systems can be traced back to the Korean War [1]. Although, primarily due to their low cost, nylon and E-glass fibers are still being used today; high-performance polymeric fibers (typically used in the form of woven fabrics or cross-plied collimated uni-directional filaments) are now the standard in most fiber-reinforced body-armor applications.

The high-performance polymeric fibers used today are characterized by substantially improved strength, stiffness and energy-absorbing capacity. Among these high-performance fibers the most notable are: (a) *poly-aramids* (e.g. Kevlar®, Twaron®, Technora®); (b) highly-oriented *poly-ethylene* (e.g. Spectra®, Dyneema®); (c) *poly-benzobis-oxazole*, PBO (e.g. Zylon®), and (d) *poly-pyridobisimi-dazole*, PIPD (e.g. M5®). When tested in tension, all these materials differ significantly from the nylon fibers, having very high absolute stiffness, extremely high density-normalized strength, and quite low (<4%) strains-to-failure. These fibers essentially behave, in tension, as rate-independent linear elastic materials. When tested in transverse compression, however, these fibers are similar to nylon and can undergo large plastic deformation without a significant loss in their tensile load-carrying capacity. This behavior is quite different from that found in carbon or glass fibers, which tend to shatter under transverse compression loading conditions.

Over the past two decades, there has been a great deal of work done on understanding the mechanical behavior of fabrics based on the high-performance fibers which are extensively employed in a variety of ballistic and impact protection applications. Nevertheless, the design of fabric-armor systems remains largely based on the employment of extensive experimental test programs, empiricism and old practices. While such experimental programs are critical for ensuring the utility and effectiveness of these systems, they are generally expensive, time-consuming and involve destructive testing. Consequently, there is a continuing effort to reduce the extent of these experimental test programs by complementing them with the corresponding computation-based engineering analyses and simulations. Among the main computational engineering analyses used to model ballistic performance of flexible armor, the following main classes can be identified: (a) Finite element analyses based on the use of pin-jointed orthogonal bars to represent flexible fabric yarns, [e.g. 2]; (b) More-detailed full-blown 3D continuum finite element analyses [e.g. 3]; (c) Unit-cell based approaches have been used extensively in order to derive the equivalent (smeared) continuum-level (membrane/shell) material models of textile composites from the knowledge of the meso-scale fiber and yarn properties, fabric architecture, and inter-yarn and inter-ply frictional characteristics. [e.g. 4]; and (d) The use of higher-order membrane/shell finite element analyses to represent the dynamic response of fabric under ballistic loading conditions [e.g. 5].

As pointed out above, while major efforts have been made in recent years to develop sophisticated numerical models capable of elucidating the ballistic performance of fabric armors, most of these models either lack computational efficiency or fail to capture many physical aspects of the yarn and fabric architecture and/or contact dynamic phenomena. Hence, in our recent work [6], a new meso-scale unit-cell based material model for a single-ply plain-woven Kevlar® 129 fabric was developed in order to address some of the shortcomings of the models listed above. The main objective of the present work is to utilize our model in a series of computational analysis of prototypical multi-ply flexible mat body armor.

2. OVERVIEW OF THE MESO-SCALE MATERIAL MODEL [6]

Prior to the overview of the material model in question, the following two terms are clarified: (a) "*meso-scale*" is used to denote yarn-level millimeter length scale details of the fabric microstructure/architecture. In other words, finer-scale molecular-level and fiber-level material details are not considered explicitly and instead only their lumped contributions are taken into

account; and (b) "*unit-cell*" is used to denote the basic structural unit in a woven single-ply fabric so that a fabric patch can be considered as an in-plane assembly of such units.

The basic idea behind the unit-cell based approach is that the mechanical response of the fabric unit-cell (represented in terms of a number of structural members, e.g. trusses, springs, etc.) is smeared out into the equivalent response of a (anisotropic) continuum material. A simple schematic of the unit cell which is used to represent the plain-woven single-ply fabric structure/architecture allotted to a single yarn crossover is depicted in Figure 1(a). Its continuum-level material point counterpart is shown in Figure 1(b). Within the continuum-material framework, the yarns are not represented explicitly but rather by two material directions whose orientations are denoted in terms of material vectors, g_1 and g_2.

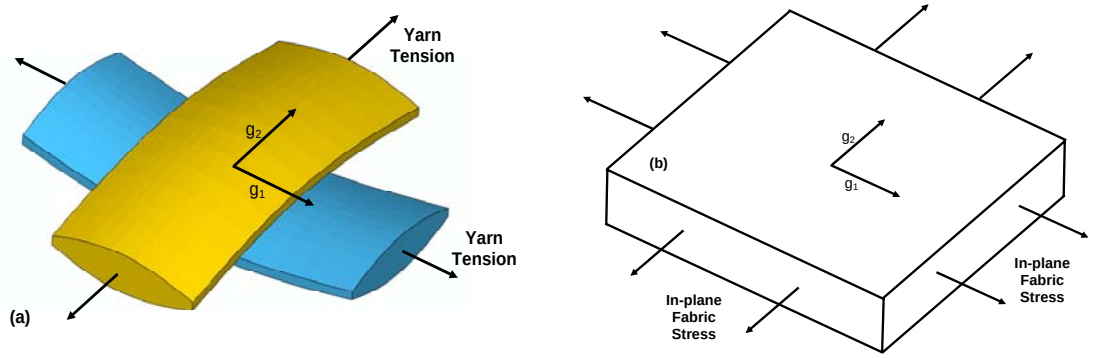

Figure 1. The relationship between a fabric unit cell (a) and the corresponding material point in an anisotropic continuum (b).

Coupling between the continuum material formulation and the unit-cell geometry/architecture and mechanical response is done in the following way: (a) the deformation state of a continuum material point (as quantified by the corresponding deformation gradient) is used to update the unit-cell geometry/architecture and the extent of yarn slip; (b) the updated unit-cell geometry/architecture and the extent of yarn slip are then used to compute the forces and moments acting on its structural members; and (c) the computed forces and moments along with their gradients through the shell thickness are next used to compute the associated stress state at the corresponding continuum material point.

It must be noted that in order for the aforementioned approach to be valid (i.e. in order for homogenization of the fabric unit-cell response to be justified), the characteristic length scale in the numerical analysis in which the model is used (e.g. the projectile and the fabric-patch sizes and the stress/strain gradient ranges in a projectile/fabric impact problem analyzed in the present work) must be large in comparison to the fabric unit-cell edge length.

2.1 Fabric Unit Cell Geometry/Architecture The geometry/architecture of the plain-woven single-ply fabric unit-cell used in the present work is displayed in Figure 2. The warp and weft yarn segments within the unit-cell are each represented using two-member truss elements. To represent the yarn crimp arising from yarn weaving into the fabric, the truss elements do not lie in the plane of the fabric. Warp and weft yarn segments cross each other and interact at the crossover point. Yarn sliding leads to the motion of this point. To allow for yarn stretching, truss elements have finite axial stiffness but their (out-of-plane) bending stiffness is set to infinity. Yarn out-of-plane bending is modeled as rotation of the two truss members of a yarn segment at

the crossover point and the associated yarn bending stiffness is accounted for through the use of a rotational spring attached to two truss members of the same yarn at the crossover point.

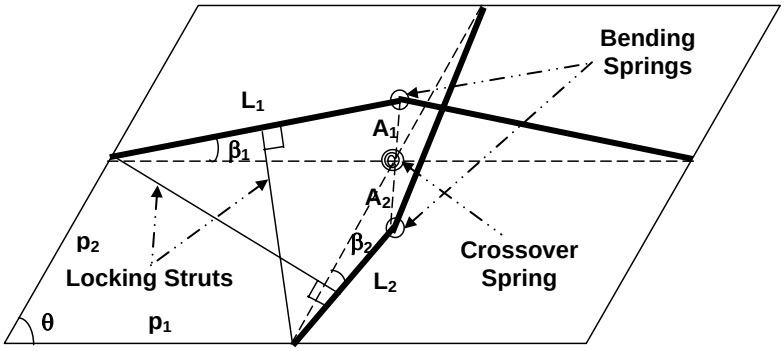

Figure 2. The geometry/architecture of a plain-woven single-ply fabric unit cell used in the present work.

Contacts and interactions between the warp and weft yarns at a crossover point in the direction normal to the plane of the fabric are modeled using a *"contact spring"* which provides elastic resistance towards the yarn crimp-amplitude reductions and the associated yarn cross-section changes.

Elastic and dissipative resistances towards the in-plane shear bending and the relative in-plane rotation of the warp and weft yarns in the presence of yarn/yarn friction are modeled using a rotational spring and a rotational damper, respectively.

Additional contacts and interactions between the warp and weft yarns can take place as a result of *"locking"*, a phenomenon which involves lateral compression (and the associated changes in the cross-sectional areas) of warp or weft yarns by the surrounding adjacent yarns of the other (warp or weft) family. This phenomenon can occur either as a result of a larger in-plane shear deformation (*"shear locking"*) or as a result of large uniaxial tensile loading along the axis of one yarn family *("cross locking"*). Since the unit-cell model used here does not track the yarn cross-sectional area changes, locking is modeled through the use of *"locking trusses"* which: (a) remain normal to the yarns of a given family (and, thus, the length of these trusses quantifies the distance between adjacent yarns of the same family); (b) allow the build-up of contact/locking forces between the yarns after the yarn locking conditions are met; and (c) provide increasingly higher unit-cell shear stiffness once the yarn locking conditions are met.

The geometry/architecture of the fabric unit-cell can then be described by the following 13 parameters: (a) two unit cell half edge lengths; (b) two yarn-segment/truss lengths; (c) two crimp angles; (d) two crimp amplitudes; (e) two locking truss lengths; (f) two inclination angles of the locking trusses to the fabric plane; and (g) the in-plane shear (i.e. warp-yarn/weft-yarn included) angle. Out of these 13 parameters only five are independent since simple geometrical relations exist between these parameters in a given configuration of the unit cell. The two unit-cell edge lengths, the two yarn lengths, and the in-plane warp-yarn/weft-yarn included angle, were considered as the independent variables needed to fully describe the geometry and the architecture of the unit-cell [6].

2.2 Constitutive Relations for Unit-Cell Structural Components As presented in the previous section, the fabric architecture and behavior within a unit-cell is described in terms of a number of structural elements, e.g. the two-member trusses, bending springs, contact springs, etc. In this

section, the corresponding mechanical constitutive relations are described for all the elements. These relations (defined in great details in Ref.[6]) are necessary for computation of the forces/moments acquired by these components during deformation as well as of the associated energy storage/dissipation.

Yarn-Truss Members: each yarn-truss member is described using a linear elastic relationship between yarn stretch and yarn tension. This relationship is valid until the point of yarn failure past which tension drops to zero.
Crimp Rotational Spring: Out-of-plane yarn bending is enabled through the use of a rotational spring whose constitutive relation is defined as a linear function between the crimp angle and the out-of-plane bending moment.
Yarn Contact Spring: Yarn/yarn interactions and yarn cross-sectional area changes at the crossover points are accounted for through the use of a non-linear, axial *"interference"* spring whose contact-force vs. yarn-interference relation is defined using an exponential function.
Locking Trusses: To account for the fact that during locking, yarn cross-sectional area changes are taking place primarily in the direction of the major axis of the yarn cross-section, the locking response is expected to be more compliant than the yarn crossover-interference response. Therefore, a power-law relation is used to describe the locking force vs. locking interference relationship.
In-plain Rotational Spring-Damper: Since the contribution of yarn locking at large shear angles to the fabric response has been accounted for through the use of the locking trusses, only the additional elastic (due to yarn bending at the crossover points) and dissipative (frictional losses due to yarn rotations at the crossover points) components of the in-plane fabric shear remain to be addressed. The latter are accounted for through the use of an in-series spring-damper assembly attached to the cross-over point. The moment versus rotation-angle relationship for the spring is defined using a linear elastic law, while the moment rotation-angle rate relationship for the damper is defined using a viscous-type power law.

2.3 Determination of the Current Unit-Cell Geometry and Architecture As discussed in Section 2.1, five independent geometrical parameters are needed to fully describe the current geometry/architecture of the unit-cell. In this section it is shown how are these parameters related to the continuum-level deformation state of the material point corresponding to the unit-cell in question.

At the continuum level, the state of deformation at a given material point is described by the deformation gradient, F, whose components in a Cartesian coordinate system are defined as:

$$F_{jk}(t) = \frac{dx_j(t)}{dX_k} \tag{1}$$

where $x_j(t)$ is the *j-th* component of a material point at time *t*, and X_k the *k-th* component of the same point in the initial/un-deformed configuration.

At the continuum level, the warp and the weft yarns can be described using vectors p_i *(i=1, 2)* aligned with the axis of these yarns and the length of these vectors can be set equal to the corresponding current unit-cell edge lengths, p_i *(i=1, 2)*. These vectors can be related to their initial counterparts, $p_{0,i}$ *(i=1, 2)* as:

$$\mathbf{p_i} = \mathbf{F}\mathbf{p_{0,i}} \qquad (i=1,\ 2) \tag{2}$$

The lengths of p_i *(i=1, 2)* can be defined as:

$$p_i = \sqrt{\mathbf{p_i} \cdot \mathbf{p_i}} = \sqrt{(\mathbf{F}\mathbf{p_{0,i}}) \cdot (\mathbf{F}\mathbf{p_{0,i}})} = \sqrt{\mathbf{p_{0,i}}(\mathbf{F}^{\mathbf{T}}\mathbf{F})\mathbf{p_{0,i}}} \tag{3}$$

where the yarn-included angle θ can be computed from:

$$\mathbf{p_1} \cdot \mathbf{p_2} = (\mathbf{F}\mathbf{p_{0,1}}) \cdot (\mathbf{F}\mathbf{p_{0,2}}) = p_1 p_2 \cos\theta \tag{4}$$

Under the condition that no slip occurs between yarns at the crossover point, so that the location of the crossover point is related to the unit-cell deformation in an affine manner, Eqs. (3)-(4) also represent the unit-cell edge lengths and the yarn included angle at the meso-scale unit-cell level. Thus, three unit-cell geometrical parameters, p_i *(i=1, 2)*, and θ, can be obtained from the continuum-level deformation gradient of a point associated with the unit-cell in question. The remaining two parameters, the yarn-truss lengths, L_i *(i=1, 2)*, are not defined at this point. In other words, there is an infinite number of unit-cell configurations which can be associated with a given (continuum-level) deformation state. However, different configurations will be associated with different levels of the (internal) elastic stored energy. To determine the *"unique"* unit-cell configuration associated with a given deformation state, an energy argument is used. That is, it is postulated that the unit-cell will acquire the geometry/architecture associated with a lowest level of the elastic stored energy. To determine this unique structure of the unit-cell, a standard optimization algorithm can be used, as discussed below.

Within the optimization procedure used in the present work, the *"objective function"* (i.e. the total elastic stored energy within the unit cell at a given state of deformation, as defined by the current deformation gradient) is minimized with respect to the *"design variables"* (i.e. the two truss lengths, L_1 and L_2). Toward that end, the total strain energy stored in the trusses (due to yarn extension), bending springs (due to yarn bending), and yarn-crossover spring (due to yarn-crossover contacts and bending) is first expressed as a function of the L_1 and L_2. This was done by summing the individual stored energy components, each of which is obtained by integrating the force/moment over the loading path of the structural member in question. Then starting with initial guess values for the L_1 and L_2, these two parameters are varied in a systematic manner (using an optimization algorithm) in order to determine their values which minimize the total elastic energy stored in the unit cell. Since the objective function possesses only one minimum in a realistic range of values for L_1 and L_2, a local optimization algorithm could be used. The Downhill Simplex optimization algorithm [7] was selected since it does not require the evaluation of the derivatives of the objective function which makes it computationally very efficient.

2.4 Determination of the Material-point In-plane Stress State Once the current geometry/architecture of the unit cell is determined (i.e. once L_1 and L_2 corresponding to the minimum elastic stored energy are computed), forces and moments acting on different structural members at the faces of the unit cell can be computed using the appropriate constitutive relations. These in turn, can be used to compute the in-plane stress state at the material point associated with the unit cell in question. It should be noted that the *"true"* measure of the stress

state in the deformed configuration of a material point is the Cauchy stress, σ. To compute the stress state, the following relation is used between the traction-force vector, t, resulting from σ and acting on a small surface element *dS* with a unit normal n:

$$\mathbf{t} = \mathbf{n}\sigma dS \tag{5}$$

Thus, if the forces/moments acting on each structural member of the unit cell are used to compute the traction force acting on each of the unit cell faces in the current configuration, then Eq. (5) can be used to compute the corresponding in-plane material point stresses. Using this procedure the following expression for the stress tensor at a given material point is obtained:

$$\begin{aligned}\sigma = &\frac{1}{2p_2\sin\theta}\left(T_1\cos\beta_1 - \frac{M_{b1}\sin\beta_1}{L_1} - \frac{M\cos\theta}{2p_1\sin\theta} - \frac{F_{L1}p_1}{d_1} - F_{L2}\left(\frac{p_2^2\cos^2\theta}{p_1 d_2} + \frac{p_2\sin\alpha_2|\cos\theta|\sin\beta_1}{L_1}\right)\right)(g_1\otimes g_1)\\ &+\frac{1}{2p_1\sin\theta}\left(T_2\cos\beta_2 - \frac{M_{b2}\sin\beta_2}{L_2} - \frac{M\cos\theta}{2p_2\sin\theta} - \frac{F_{L2}p_2}{d_2} - F_{L1}\left(\frac{p_1^2\cos^2\theta}{p_2 d_1} + \frac{p_1\sin\alpha_1|\cos\theta|\sin\beta_2}{L_2}\right)\right)(g_2\otimes g_2)\\ &+\left(\frac{M}{4p_1p_2\sin^2\theta} + \frac{F_{L1}p_1\cos\theta}{2p_2d_1\sin\theta} + \frac{F_{L2}p_2\cos\theta}{2p_1d_2\sin\theta}\right)(g_1\otimes g_2 + g_2\otimes g_1)\end{aligned} \tag{6}$$

where g_1 and g_2 are unit vectors aligned with the current orientation of the two yarns and symbol $\otimes$ is used to denote a tensorial product of two vectors. It should be noted that as seen in Eq. (6), the stress state at a given material point has contributions from the yarn tensions, T_i, yarn bending moments, M_{bi}, locking forces, F_{Li}, and the inter-yarn bending moment, M. Furthermore, it must be noted that Eq. (6) does not include the effect of yarn slip to the in-plane stresses. This effect is added in Section 2.6.

To summarize, the (in-plane) Cauchy stress tensor for a given unit cell is computed using the following procedure: (a) The forces that all load-bearing meso-structural members exert on the unit-cell faces are computed first; (b) The components of these forces that lie in the plane of the fabric are determined next; (c) These forces are then resolved along the yarn directions, designated by unit vectors g_i; (d) The resolved forces are next divided by the appropriate projected areas to obtain stresses and the results are expressed in tensorial form in terms of the yarn direction vectors g_i; and (e) finally, it is ensured that the resulting stress tensor is symmetric.

2.5 Out-of-plane Behavior of the Fabric The unit-cell material model developed in the previous section describes only the in-plane fabric behavior, the behavior which is dominated by in-plane stretching along the yarn directions and the inter-yarn rotation-induced in-plane shear. When plain-woven fabric is modeled using shell finite elements then, in addition to the in-plane fabric behavior, one must also define the out-of-plane fabric behavior. The out-of-plane behavior includes: (a) the through-the-thickness compression; (b) two transverse shears; (c) two out-of-plane bending modes; and (d) fabric twist deformation mode. In the remainder of this section, contributions of the six aforementioned out-of-plane deformation modes to the stress state at a given material point are presented and discussed.

Through-the-thickness Compression The through-the-thickness compression is resisted by the cross-over axial interference spring. Since the in-plane tensions/yarn-decrypting are also resisted

by the same spring, and the in-plane tensions do not induce through-the-thickness stresses, one must determine the additional compressive displacement experienced by the spring due to through-the-thickness compression before the through-the-thickness normal compressive stress can be calculated (by dividing the additional contact force by the current unit-cell surface area).
Transverse Shear Within ABAQUS/Explicit finite element program [8] used in the present work, only a linear-elastic transverse shear response of the fabric can be defined. This requires specification of two transverse shear stiffness moduli which is done within the main finite-element model/analysis input file.

Out-of-plane Bending Since within the VUMAT User Material Subroutine, the stress state is assessed for each shell element at a number of material points with equal in-plane coordinates and different through-the-thickness locations, the effect of out-of-plane bending is (at least partly) accounted for by the in-plane material model developed in the previous section. That is, the effect of bending-induced through-the-shell-thickness tension gradient is included in the in-plane fabric response. However, the effect of the fabric's principal curvatures within the given unit cell is not taken into account. The effect of shell curvature is accounted for by determining the contribution of the associated out-of-plane bending moments (defined as a linear function of the principal curvatures) to the stress state for all material points of a given shell element. The principal curvatures are computed using the through-the-thickness gradient of the corresponding in-plane normal strains.

Fabric Twist Deformation Mode While the pure out-of-plane bending discussed above is associated with a through-the-thickness gradient of in-plane normal tensile strains, fabric twist is caused by the through-the-thickness gradient in the in-plane shear strain. The effect of fabric twist is accounted for by determining the contribution of the associated out-of-plane twist moment (defined as a linear function of the twist angle) to the stress state for all material points of a given shell element. The twist angle is computed using the through-the-thickness gradient of the in-plane shear strains.

2.6 Yarn Slip at the Crossover Points The meso-scale unit-cell based material model for plain-weave fabric presented in the previous two sections was based on an assumption that no yarn slip takes place at the yarn/yarn crossover points. This assumption leads, in general, to an over-estimation of the stress levels (in highly stressed fabric regions) by the unit-cell model relative to the stress levels obtained in computational analyses in which yarns and their weaving/crimp are represented explicitly. In the latter analyses, slip of yarns at the crossover points is generally found to make significant contributions to the deformation response of fabric during impact with a high-velocity projectile. Slip of a yarn at the crossover point is caused by differences in the tension along the length of that yarn. Differences in the yarn-slip velocities at three adjacent crossover points of a yarn, lead to differences in the velocities at which the yarn material enters and leaves the unit cell associated with the middle crossover point. The latter differences give rise to a change in the un-loaded length of the yarn segments allotted to the unit cell in question. The rate of change of this length scales with the gradient of the yarn axial velocity. The yarn axial velocity, in turn, scales with the tension gradient along the yarn length via a viscous-type power-load relationship. Thus, by integrating the rate of change of the un-loaded length of the yarn segments allotted to the unit cell, temporal evolution of this length can be tracked and its current value used in the calculation of yarn tension. The slip-corrected yarn tensions are then used in Eq. (6) to compute the stress state at a material point.

2.7 Fabric Buckling The fabric unit-cell model under consideration in Figure 2 is stable only under tension even when it is constrained to remain planar. When subjected to compression, the fabric unit cell is unstable and can, in general, buckle in one of the two following modes: (a) yarns can undergo bending at the crossover points and increase their crimp (*"yarn buckling"*); or (b) the yarns can rotate about axes perpendicular to the fabric plane, causing a shearing motion of the fabric (*"shear buckling"*). To prevent buckling, rotational-inertia resistance is added explicitly to the unit-cell structural members. This procedure introduced additional reaction forces and moments which were added to their static counterparts and used in the calculation of the material point stress state.

2.8 Failure of Yarns Yarn failure is assumed to be load controlled, i.e. a yarn is broken instantaneously when its tensile load reaches or exceeds a critical value. The level of tensile load within a yarn is considered to be affected by the extent of crimp in the yarn in question and by the failure status of the contacting yarn.

2.9 Parameterization of the Material Model Before the meso-scale unit cell model developed in Ref.[6] could be used, it had to be parameterized for the fabric of interest (a Kevlar ®129 based plain-woven fabric, in the present work). This was done in Ref.[6] through the use of various sources of data such as: (a) yarn properties; (b) the results of experimental tests such as the compression tests of fabric stacks, the shear-frame test in which a square patch of the fabric (with the yarns running in the $\pm 45^{o}$ directions) is clamped along the four edges and pulled in the diagonal direction, the three-point bending and twist tests of fabric patches, etc. and ; (c) the results of simple mechanical-test finite element analyses of a finely meshed fabric unit cell. A summary of the meso-scale unit-cell based material model parameters used in the present work can be found in Table 1, Ref.[6].

2.10 Material Model Implementation in a User-material Subroutine The meso-scale unit-cell based material model is next implemented in the material user subroutine, VUMAT, of the commercial finite element program ABAQUS/Explicit [8]. This subroutine is compiled and linked with the finite element solver and enables ABAQUS/Explicit to obtain the needed information regarding the state of the material and the material mechanical response during each time step, for each integration point of each element. The essential features of the coupling between the ABAQUS/Explicit finite-element solver and the VUMAT Material User Subroutine can be summarized as follows: (a) The corresponding previous time-increment stresses and material state variables as well as the current time-step deformation gradient are provided by the ABAQUS/Explicit finite-element solver to the material subroutine. In the present work truss lengths, and yarn failure and element deletion status flags were used as the state variables; and (b) Using the information provided in (a), and the meso-scale unit-cell user material model presented in the previous section, the material stress state as well as values of the material state variable(s) at the end of the time increment are determined within the VUMAT and returned to the ABAQUS/Explicit finite-element solver. In addition, the changes in the total internal and the inelastic energies (where appropriate) are computed and returned to the solver. It should be also noted that due to the presence of in-plane and out-of-plane gradient terms in the material model, global three-dimensional matrices containing tension, normal in-plane strains or shear in-plane strains had to be assembled and used during each call of the VUMAT subroutine. Furthermore within the VUMAT, only the normal and shear in-plane and through-the-shell-thickness compression responses of the material are computed. Transverse shear stiffness of the shell elements has to be defined as part of the overall FEM model definition outside the VUMAT.

3. VALIDATION OF THE MATERIAL MODEL

To validate the model, a simple problem involving the impact of a spherical projectile onto a single-ply plain-woven fabric patch is analyzed. The initial configurations of the projectile/armor finite-element systems analyzed here are shown in Figures 3(a)-(b). In Figure 3(a), the fabric is modeled using a single layer of shell elements in which the fabric is represented using the meso-scale unit-cell based model (*unit-cell based FEM analysis*). In Figure 3(b), fabric is modeled using explicit representation of the yarns and their weaving and standard orthotropic material properties for Kevlar ®129 are used (*yarn-level FEM analysis*). Since the yarn-level analyses is inherently more accurate (but computationally quite more expensive) than the unit-cell based analyses it is used, in place of experiments, for the material-model validation. Towards that end, parallel runs of the projectile armor impact problem are carried out under different fabric-edge boundary conditions (clamped, free) and under different yarn-yarn and projectile/fabric frictional conditions using the two types of analyses. A comparison of the corresponding results is then used to test the validity of the proposed model. When comparing the results of two analyses the following two aspects are given particular attention; (a) The residual velocity of the projectile after the projectile has successfully penetrated the armor and (b) the extent, the temporal evolution and the spatial distribution of fabric-armor deformation and damage. In addition the contributions of the three main mechanisms (yarn strain energy, yarn kinetic energy and the energy lost due to frictional sliding) to the energy absorbing capacity of the fabric are also closely examined.

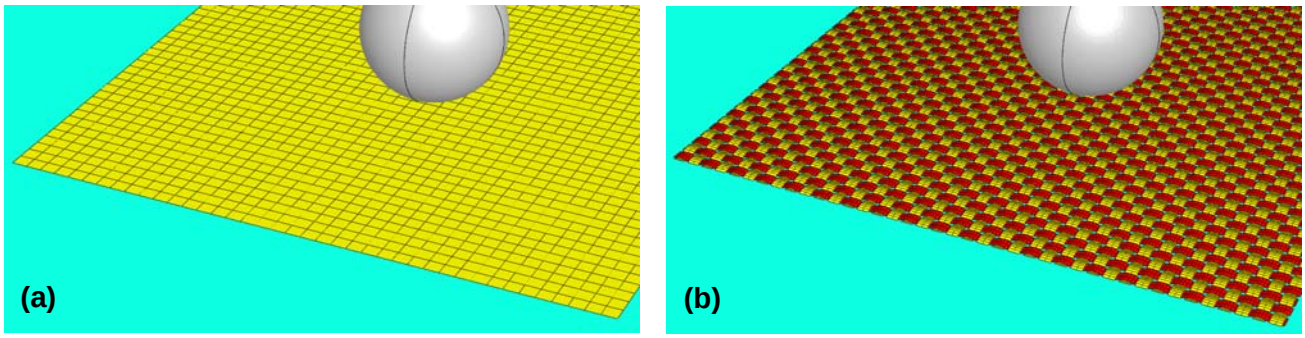

Figure 3. The initial configurations of the projectile/armor finite-element systems

While in Ref.[6] a comprehensive presentation of the results obtained using the two types of FEM analyses was given, only few selected results are included here. The first set of results is displayed in Figures 4(a)-(d) and 5(a)-(d) for the yarn level and the unit-cell based analyses respectively. These results were obtained under clamped boundary conditions being applied to all four edges of the fabric patch and at a value of the yarn/yarn and projectile/fabric frictional conditions of 0.5. When a projectile hits the armor, two elastic-stress waves are generated: (a) a longitudinal wave which travels away from the point of impact along the principal yarns (the yarns directly hit by the projectile) and along those secondary yarns (the yarns not directly impacted by the projectile) which are interacting with the principal yarns. Propagation of the longitudinal wave outward from the point of impact enables a large fraction of the fabric armor to undergo deformation and, thus, absorb the kinetic energy of the projectile; and (b) a transverse wave which propagates outward from the point of impact at a velocity substantially lower than the sound speed and is responsible for stretching of the principal and the *"engaged"* secondary yarns. In the two analyses the temporal and spatial evolutions of the longitudinal-wave front

were found, as expected, to be quite comparable. On the other hand, the temporal evolution and the spatial distribution of the transverse-wave front are, in general, affected to a greater extent by yarn/yarn interactions. Therefore, a comparison of the transverse-deflection wave-front propagation results obtained using the two FEM analyses (Figures 4(a)-(d) and 5(a)-(d)) can be considered as a good validity test for the meso-scale unit-cell based material model developed in the model under consideration.

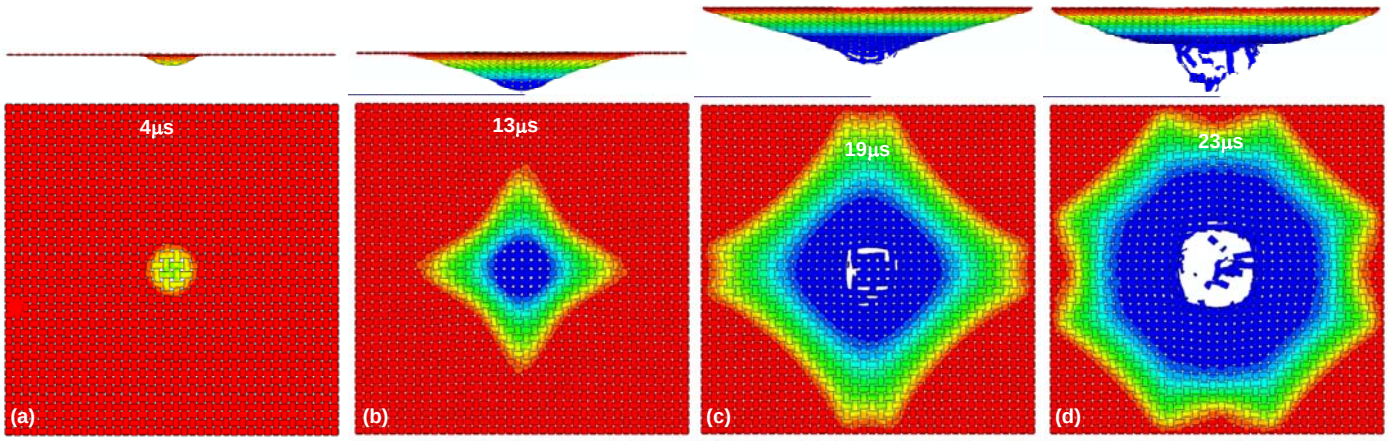

Figure 4. The temporal evolution of deformation in the fabric for the yarn-level FEM model under the yarn/yarn $\mu_{y/y}$ and projectile/fabric $\mu_{p/f}$ friction coefficients of 0.5. Contour bands correspond to different values of the transverse displacement, i.e. the displacements normal to the fabric surface. All four fabric edges are fixed.

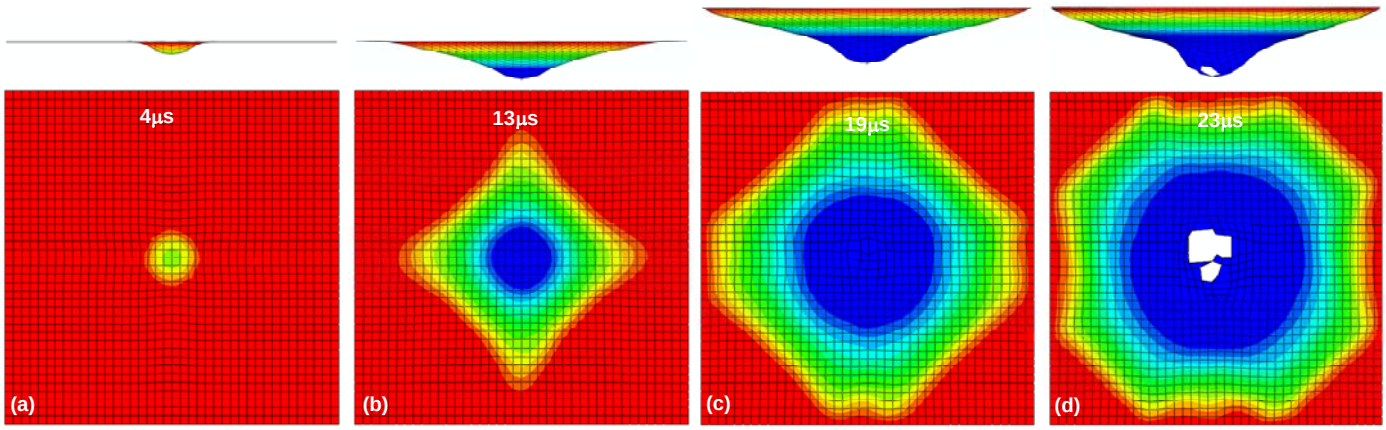

Figure 5. The temporal evolution of deformation in the fabric for the unit-cell based FEM model under the yarn/yarn $\mu_{y/y}$ and projectile/fabric $\mu_{p/f}$ friction coefficients of 0.5. Contour bands correspond to different values of the transverse displacement, i.e. the displacements normal to the fabric surface. All four fabric edges are fixed.

In Figures 4(a)-(d) and 5(a)-(d), side and top views of the fabric along with superimposed contour plots of the transverse displacement (the displacement normal to the fabric surface) are shown. A simple comparison of the results displayed in these figures reveals that the temporal evolution of the deformation state of fabric is quite similar in the two analyses and can be summarized as follows: (a) Initially, the shape of the transverse-deflection wave-front in the fabric is nearly circular in both analyses and, thus, essentially identical to the shape of the projectile/fabric contact-zone, Figures 4(a)-(d) and 5(a)-(d); (b) In the case of the yarn-level FEM analysis, as the time proceeds, the transverse-deflection wave generated within the

principal yarns (the yarns which are in direct contact with the projectile) propagates outward and, through their interactions with the secondary yarns (the yarns which are not in direct contact with the projectile), at the yarn crossovers, cause the secondary yarns to also deflect in the transverse direction. Consequently, the transverse-wave front begins to acquire a near square shape (with the square diagonals extending in the warp-/weft-yarn directions), with the square center coinciding with the impact-zone center, Figures 4(b)-(c). In the case of the unit-cell based FEM analysis, the fabric is modeled as a continuous surface and, hence, the transverse wave can propagate in all in-plane directions from its source point (i.e. from the point of initial impact). However, since the in-plane load transfer is carried out via the yarn trusses, the transverse wave-front still acquires a square-like shape Figures 5(b)-(c); (c) The extent of the transverse wave-front propagation and the magnitudes of the corresponding deflections are quite comparable in the two FEM analyses; (d) Upon reaching the clamped edges of the fabric, the square-shaped transverse-deflection wave-front is reflected back towards the center of the impact zone and the wave front acquires an octagonal shape, Figures 4(d) and 5(d); (e) The first evidence of fabric failure is seen in the case of the yarn-based FEM analysis, Figure 4(c). In the case of the unit-cell based FEM analysis, yarn failure occurs at approximately equal post impact time, Figure 5(c). It should be noted that the agreement between the results displayed in Figures 4(c) and 5(c) is better than it appears. In Figure 5(c) yarn failure in one direction has taken place in a number of finite elements, however these elements were not deleted, as element deletion criterion requires yarn failure in two directions; (f) The final fabric penetration-hole size appears to be smaller in the case of unit-cell analysis, Figure 5(d), than in the yarn-level based case, Figure 4(d). This apparent discrepancy can be related to the element-deletion criteria used in the present work, as discussed in point (e); (g) At ~25-27μs, the projectile completely penetrates the fabric and continues to move at a residual velocity of 290.2m/s in the case of yarn-level FEM analysis and at a velocity of 289.2m/s in the case of unit-cell based FEM analysis; and (h) It should be noted that despite the fact that the projectile/fabric model has two vertical planes of symmetry, the damage region is slightly asymmetric in both types of analyses. The reason for this is that the finite-element discretization of the projectile into tetrahedron elements did not possess two planes of symmetry. The results displayed in Figures 4(a)-(d) and 5(a)-(d) thus also reveal the effect of small geometrical perturbations in the (spherical) projectile on the fabric failure response.

The level of agreement between the corresponding results displayed in Figures 4(a)-(d) and 5(a)-(d) was also observed under different boundary conditions applied to the fabric edges, different yarn/yarn and projectile/fabric frictional conditions, different projectile sizes and initial velocities and different sizes of the fabric patches and initial crimp extents in the fabric.

Temporal evolution of the reduction in the projectile kinetic energy and in the absorbed-energy components associated with the three main energy absorbing mechanisms (i.e. yarn strain energy, yarn kinetic energy and frictional-sliding losses) obtained using the two FEM analyses are displayed in Figures 6(a)-(b). These results were obtained under the same projectile, fabric, initial and boundary conditions as those displayed in Figures 4(a)-(d) and 5(a)-(d).

In Figures 6(a)-(b) the quantities displayed along the vertical axis are all normalized by the corresponding maximum projectile energy loss. Also, the residual projectile velocities are indicated and their comparison suggests a quite good agreement between the corresponding values obtained using the two analyses. A simple comparison of the results displayed in Figures 6(a)-(b) reveals that: (a) While frictional sliding in general makes a relatively minor contribution

to the overall energy absorption capacity of the system, a somewhat larger contribution of the frictional-sliding losses is present in the case of the yarn-level based analysis, Figures 6(a)-(b). This finding is consistent with the fact that, in the case of the unit-cell based analysis, yarn/yarn friction is not included explicitly and does not contribute to the frictional-sliding losses; (b) The yarn strain-energy and the yarn kinetic energy contributions to the energy-absorbing capacity of the fabric predicted by the two FEM analyses are quite comparable; (c) The full-penetration time (defined as a time when the projectile reaches its final velocity) as predicted by the two FEM analyses are comparable; (e) As the projectile begins to interact with the fabric, the contributions of yarn straining to the energy-absorption process increases. Once the projectile starts to penetrate the armor, further yarn straining ceases to occur. At the same time, the relative kinetic energy component of the yarns increases (due to yarn recoiling) and likewise the frictional-sliding component of the total yarn energy increases; and (f) The extent of agreement between the two FEM analyses regarding the energy absorption capacity of fabric under the projectile velocity of 300m/s as seen in Figures 6(a)-(b) was also observed under different initial projectile velocities.

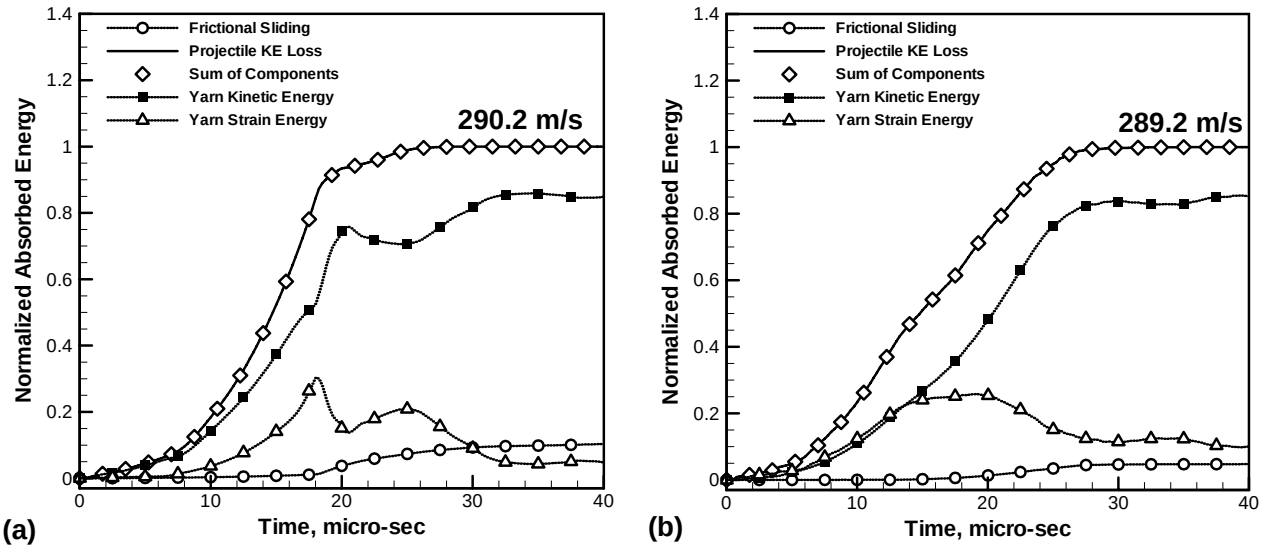

Figure 6. The temporal evolution of the absorbed projectile kinetic energy and of the three main energy absorption components (i.e. yarn strain energy, yarn kinetic energy and frictional-sliding losses) as predicted by: (a) the yarn-level FEM analyses and (b) the unit cell based FEM analyses.

4. APPLICATION OF THE MATERIAL MODEL IN THE ANALYSIS OF PERSONNEL PROTECTION

4.1 Problem Definition: A bullet-resistant vest typically consists a of front and a rear flexible mat, both made of multiple cross-stitched layers of ballistic fabric and housed within a carrier made of conventional garment material. According to the National Institute of Justice (NIJ) specification "*Ballistic Resistance of Personal Body Armor NIJ Standard–0101.04*", the highest level of protection offered by soft body armor is level III-A. Additional protection is attained in vests with front and rear pockets for the accommodation of ceramic, metallic, or high-performance polymer-fiber "*rifle*" plates. In the present work, the material model reviewed in the

previous section has been utilized to carry out a series of computational analyses aimed at assessing the ballistic performance of (rifle-plate free) soft body armor employing Kevlar© 129 based flexible mats. These mats consist of multiple stitched fabric layers interlaced with thin plastic films for added flexibility.

The results obtained in the previous section clearly revealed that the ballistic performance of a single-layer fabric is greatly affected by the nature of the boundary conditions as well as by the presence/absence and stiffness/compliance of a backing support structure. Consequently, to properly assess the response of the protective system, a simple model of a representative upper torso was introduced as the backing support structure. The effect of the fabric carrier was modeled implicitly through the use of distributed pressure loading over the surface of the fabric plies. The ballistic performance was assessed against a 9mm full metal jacketed (FMJ) round nose bullet with a nominal mass of 8.0g and fired at an initial velocity of 332m/s (a NIJ level II-A threat). Typical exploded and detailed views of the bullet/vest/upper-torso model in its initial configuration are displayed in Figures 7(a)-(b), respectively.

To represent the human body compliance, the upper torso is modeled as a deformable shell structure. In addition, four Cartesian and four Cardan connectors with nonlinear elastic and damping behavior are inserted between four nodes around the sternum area and four nodes belonging to the back of the upper torso. The effect of the lower torso is accounted for by adding one mass element and one rotary-inertia element which were coupled with the lower edge of the upper torso. The center 160mm by 160mm chest region which may experience the largest effect of the bullet strike is meshed using 2mm square elements. The rest of the upper chest is meshed using coarser three- and four-node elements with a typical edge length of 5-7mm. To obtain seamless connection between the two regions, a set of multi-point kinematic constrains are applied along the boundary separating the two regions. Typically, the upper torso contained around 9000 elements. The elastic material properties for the shell elements of the upper torso and the connector properties where taken from Ref. [9].

The soft-body flexible chest mat is also modeled using shell elements. However, the mat was divided into three sections: (a) the innermost 20-layer thick 50mm by 50mm square section containing the meso-scale unit-cell based material model developed in the present work; (b) a 100mm by 100mm outer square frame containing only the elastic portion of the fabric model used in the innermost region. Regions (a) and (b) are meshed using 1mm square elements; and (c) a coarsely meshed single-layer outer region containing three- and four-node elements with a typical edge length of 5-7mm. Typically, the chest mat contained 220000 elements. The outer region was filled with the same elastic material as region (b). Again, to ensure continuity, multi-point kinematic constraints were applied along the boundaries separating the finely meshed and the coarsely meshed regions. In addition, the outer boundary of the 100mm by 100m region is assumed to coincide with the cross-stitching lines in the mat. To mimic the effect of cross stitching, multipoint kinematic constraints were also applied to the corresponding (“stacked”) nodes of all the layers through the thickness of the mat. The thin plastic sheets separating adjacent layers in the mat were not modeled explicitly. Rather, their effect was included implicitly by adjusting the value of the inter-layer friction coefficient.

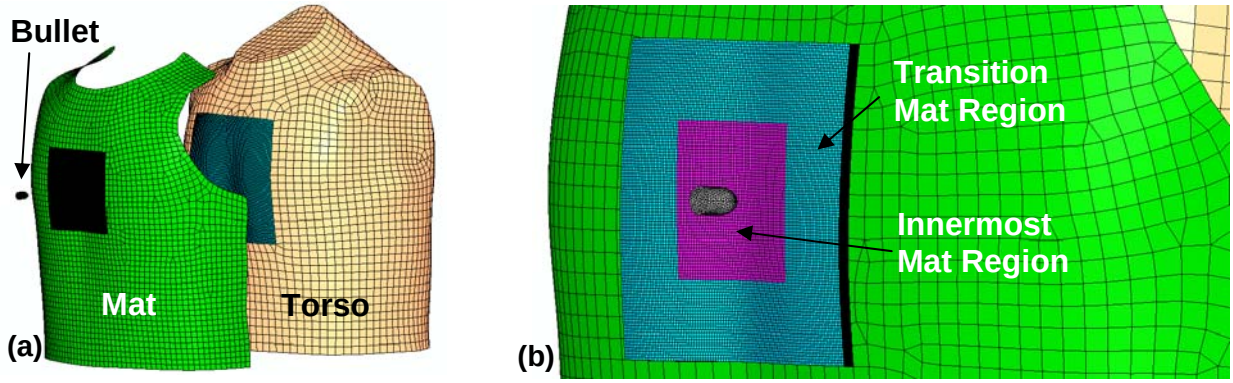

Figure 7. The initial configuration of the bullet/chest mat/upper-torso model: (a) an exploded view; and (b) a detailed view of the impact region

The bullet was meshed using tetrahedron elements with an average edge length of 1mm. Typically, the copper jacket region contained 3000 elements while the lead core region contained 3000 elements. The jacket and the core share nodes along their contact surface, i.e. a perfect jacket/core interfacial bonding is assumed. Details regarding the material models for copper and lead based on a linear equation of state, the Johnson-Cook strength model, the Johnson-Cook failure model and an erosion algorithm based on the maximum allowable instantaneous geometrical strain used in the present work can be found in Ref. [10].

Interactions between the projectile, armor mat layers, and torso were modeled using a *"Hard Contact Pair"* type of contact algorithm. Within this algorithm, contact pressures between two bodies are not transmitted unless the nodes on the *"slave surface"* contact the *"master surface"*. No penetration/over-closure is allowed and there is no limit to the magnitude of the contact pressure that could be transmitted when the surfaces are in contact. Transmission of shear stresses across the contact interfaces is defined in terms of a static, μ_{st}, and a kinematic, μ_{kin}, friction coefficient and an upper-bound shear stress limit, τ_{slip} (a maximum value of shear stress which can be transmitted before the contacting surfaces begin to slide).

To prevent hourglassing effects which may arise due to the use of reduced-integration elements, a default value of hour-glass stiffness was used. No mass-scaling algorithm was used to increase the maximum stable time increment.

Computational analyses were run on a machine with two 2.33GHz Quad-core Intel Xeon processors with 16GB of RAM. A typical computational analysis run to the point when either the bullet is defeated of the soft body-armor mat is fully penetrated required between two and three hours of (wall-clock) time.

4.2 Representative Results: A bullet-resistant vest not only has to stop a bullet but also has to prevent excessive intrusion of its back layers into the wearer's body at the point of impact. Otherwise, localization of the impact to a small area may cause severe internal injuries. To achieve this function, soft body armor must be capable of mitigating blunt trauma by distributing the localized impact loading over a large portion of the torso. The ability of the flexible protection to fulfill these functions is investigated in the present work. Specifically, the computational analysis described in Section 4.1 and the material model overviewed in Section 3 enabled investigations of: (a) the energy absorbing capacity of the personnel protection system needed to stop a projectile; and (b) the ability of personnel protection system to minimize blunt trauma caused by excessive intrusion of its back layers into the wearer's torso and highly

localized impact loads. Since this portion of the work is in its early stages, only a few representative results will be shown and discussed in this section. However, the long term goal of this work is to develop computational capabilities which will enable full-scale design, optimization, and performance validation of personnel protection systems.

A set of examples of the results obtained in this portion of the present work is displayed in Figures 8-11. The final deformed shape of the defeated 9mm-caliber round nose projectile is displayed in Figure 8. Plastic deformation of the projectile has been found to be a significant energy absorbing mechanism capable of absorbing between 10and 20% of the projectile kinetic energy. The partially penetrated soft-armor mat region has been displayed in Figure 9. It is generally found that buildup of the strain energy and acquisition of the kinetic energy by different layers of the soft-armor mat both act as important mechanisms for absorption of the projectile kinetic energy. The absolute magnitudes of these absorbed-energy components is found to be significantly affected by the extent of projectile/mat-layer and inter-layer friction in a way similar to that described in Section 3. A more comprehensive investigation of the role of friction is underway.

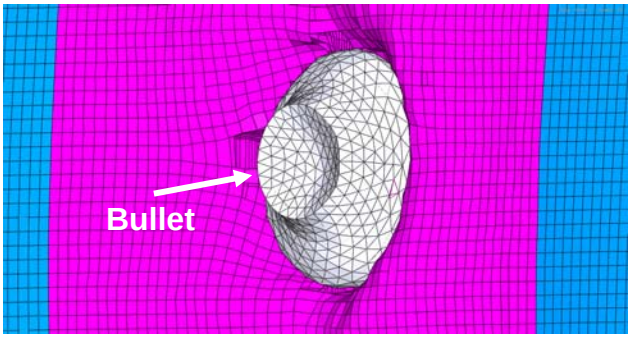

Figure 8. Final deformed shape of a defeated 9mm round-nose bullet

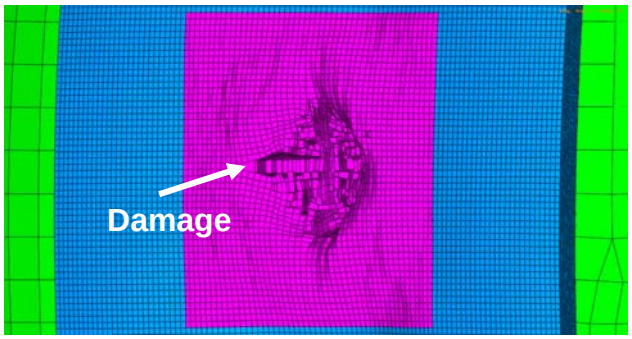

Figure 9. Spatial distribution of the post-impact damage within the soft body armor mat

Temporal evolution of the x-component of displacement of a node in the center portion of the sternum (a measure of the chest intrusion) is displayed in Figure 10. The positive x-direction coincides with the direction of projectile motion. The maximum chest intrusion is found to be significantly affected by cross stitching of the flexible vest. This finding was subsequently related to a cross-stitching induced increase in soft body armor mat transverse stiffness. It should be noted that in the present formulation the behavior of the torso is nearly perfectly elastic. In other words, energy dissipation is achieved only through frictional losses at the torso/vest interface and within the 4 sternum connectors. This affects the results displayed in Figure 10 in at least 2 ways: (a) the maximum intrusion is quite small (ca. 0.09mm); and (b) the intrusion is reversible and oscillatory. A more advanced model for the torso will be used in our future work.

The distribution of surface pressures corresponding to the maximum torso-intrusion condition is displayed in Figure 11. It should be noted that, for improved clarity, the armor vest is not displayed in Figure 11 and that the results displayed correspond to a case when the torso was rigidized (except for the 160mm by 160mm center region). As explained earlier, spreading of the impact load over a wider portion of the chest is an important functional requirement of soft body armor. The results displayed in Figure 11 clearly show that impact loads are indeed spread over a wide region of the sternum. This can be seen by comparing the defeated projectile (displayed in Figure 11) with the size of the region of the sternum subject to considerable surface loads.

As discussed earlier, application of the current computational procedure and material model to analyze the ballistic protection performance of soft body armor is in its early stages. Nevertheless, the preliminary results are encouraging and suggest that the procedure can be brought to the level that large-scale design, optimization and performance validation of body-armor vests is feasible. The multi-disciplinary optimization framework needed has been recently developed by the present authors [11] in will be utilized in our future work.

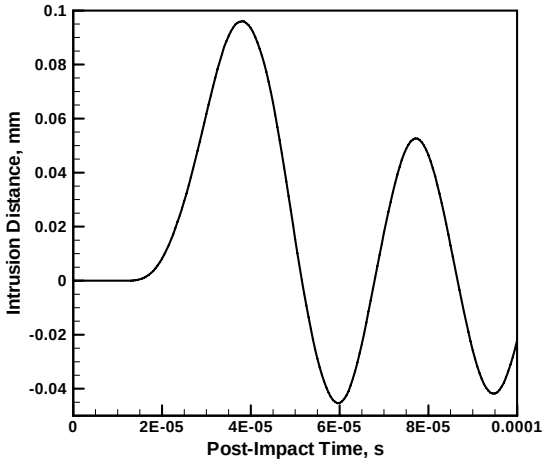

Figure 10. Temporal evolution of the torso intrusion by the back layer of the vest

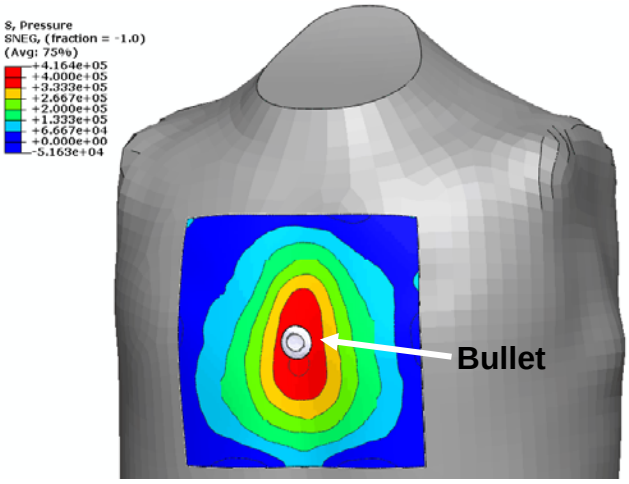

Figure 11. Spatial distribution of the surface pressure corresponding to the maximum torso

5. SUMMARY AND CONCLUSIONS

Based on the material-model development procedure overviewed and the results of the subsequent computational analyses, the following main summary remarks and conclusions can be drawn:

1. A simple meso-scale unit-cell based material-model for plain-woven single-ply fabric armor developed in Ref [6] is overviewed, implemented in a User-material Subroutine, and linked with the commercial explicit finite element program ABAQUS/Explicit.

2. The material model is next validated by caring out a series of transient non-linear dynamics finite-element analyses of impact of a single-layer fabric by a high-speed spherical steel projectile and by comparing the results with their counterparts obtained in the corresponding computational analyses in which yarns and their weaving is represented explicitly

3. The validation procedure described in point 2 revealed that, in general, the proposed material model for the plain-woven single-ply fabric can reasonably well account for the fabric behavior when subjected to ballistic impact loading.

4. To demonstrate the full utility of the present model, the model is used in a full scale computational investigation of impact into a personnel protection system chest mat placed in contact with a flexible structure mimicking a human torso.

6. ACKNOWLEDGEMENTS

The material presented in this paper is based on work supported by the U.S. Army/Clemson University Cooperative Agreements W911NF-04-2-0024 and W911NF-06-2-0042. The authors are indebted to Dr. Fred Stenton for the support and a continuing interest in the present work.

7. REFERENCES

1. **R. E. Wittman and R. F. Rolsten,** *"Armor of Men and Aircraft***", 12th National SAMPE Symposium, SAMPE, 1967.**
2. **D. Roylance and S. S. Wang,** *"Penetration Mechanics of Textile Structures, Ballistic Materials and Penetration Mechanics***," Amsterdam: Elsevier, 1980, 273–292.**
3. **Y. Duan, M. Keefe, T. A. Bogetti and B. A. Cheeseman,** *"Modeling Friction Effects on the Ballistic Impact Behavior of a Single-ply High-strength Fabric***," International Journal of Impact Eng., 31, 2005, 996–1012.**
4. **M. J. King, P. Jearanaisilawong and S. Socrate,** *"A Continuum Constitutive Model for the Mechanical Behavior of Woven Fabrics***," International Journal of Solids Struct., 42, 2005, 3867-3896.**
5. **B. R. Scott and C. F. Yen**, *"Analytic Design Trends in Fabric Armor,"* **Proceedings of the 22nd International Ballistics Symposium, 2005, 752-760.**
6. M. Grujicic, W. C. Bell, T. He and B. A. Cheeseman , "A Meso-Scale Based Dynamic Material Model for Plain-Woven Single-Ply Fabric", Journal of Material Science, submitted for publication, April 2008.
7. **Simplex Numerical Recepties**
8. **ABAQUS Version 6.7.4, User Documentation, Dassault Systems, 2007.**
9. **ABAQUS Version 6.7.4, Example Problems Manual, "3.3.1 Seat Belt Analysis of a Simplified Crash Dummy", Dassault Systems, 2007.**
10. **M. Grujicic, B. Pandurangan, U. Zecevic, K. L. Koudela and B. A. Cheeseman,** *"Ballistic Performance of Alumina/ S-2 Glass-Reinforced Polymer-Matrix Composite Hybrid Lightweight Armor Against Projectiles"*, **Multidiscipline Modeling in Materials and Structures, 3, 2007, 287-312.**
11. **M. Grujicic, V. Sellappan, G. Arakere, J. C. Ziegert, F. Y. Koçer and D. Schmueser,** *"Multi-Disciplinary Design Optimization of a Composite Car Door for Structural Performance, NVH, Crashworthiness, Durability and Manufacturability"***, Multidiscipline Modeling in Materials and Structures, accepted for publication, December 2007.**

Filename: SAMPE_2008_M026.doc
Directory: C:\Documents and Settings\micag\Desktop\RESEARCH\01 ARL Aberdeen\06 FLEXIBLE_ARMOR\05 SAMPE
Template: C:\Documents and Settings\micag\Application Data\Microsoft\Templates\Normal.dot
Title: REACTOR-SCALE MODELING OF CHEMICAL VAPOR DEPOSITION
Subject:
Author: Mica Grujicic
Keywords:
Comments:
Creation Date: 5/22/2008 1:11:00 PM
Change Number: 8
Last Saved On: 5/22/2008 2:04:00 PM
Last Saved By: Clemson University
Total Editing Time: 7 Minutes
Last Printed On: 8/7/2008 6:38:00 PM
As of Last Complete Printing
Number of Pages: 18
Number of Words: 8,349 (approx.)
Number of Characters: 47,592 (approx.)